



HAL
open science

Some aspects of the magnetomechanical coupling in the strengthening of nonoriented and grain-oriented 3% SiFe alloys

E. Hug, Olivier Hubert, M. Clavel

► **To cite this version:**

E. Hug, Olivier Hubert, M. Clavel. Some aspects of the magnetomechanical coupling in the strengthening of nonoriented and grain-oriented 3% SiFe alloys. *IEEE Transactions on Magnetics*, 1997, 33 (1), pp.763-771. 10.1109/20.560110 . hal-01560743

HAL Id: hal-01560743

<https://hal.science/hal-01560743>

Submitted on 11 Jul 2017

HAL is a multi-disciplinary open access archive for the deposit and dissemination of scientific research documents, whether they are published or not. The documents may come from teaching and research institutions in France or abroad, or from public or private research centers.

L'archive ouverte pluridisciplinaire **HAL**, est destinée au dépôt et à la diffusion de documents scientifiques de niveau recherche, publiés ou non, émanant des établissements d'enseignement et de recherche français ou étrangers, des laboratoires publics ou privés.

Some aspects of the magnetomechanical coupling in the strengthening of non oriented and grain oriented 3% SiFe alloys

E. Hug, O. Hubert and M. Clavel*

Abstract - An investigation has been carried out on the effect of plastic strains on the magnetic properties of grain oriented and non oriented 3%SiFe alloys. A drastic degradation of these properties with increasing deformations is observed for magnetic field amplitudes ranging between 0 and 2000 A/m. Empirical relationships between plastic strain and magnetic characteristics are obtained. Materials exhibit a Lüders strain state under tensile loading in a low plastic deformation range. Meanwhile, the classical Ramberg-Osgood law is verified. The observation of the dislocation features at various plastic strain levels shows three typical configurations : hexagonal cells in the Lüders strain state, small tangles and isolated screw dislocations at medium values of strain, and finally high density tangles at higher deformations. In the same way, the densities of main and secondary magnetic domains follow an evolution in three stages with increasing strains. It is shown that the transverse domain patterns take place to counterbalance the increase of magnetoelastic energy due to the strengthening. The evolution of the coercivity and the initial relative permeability with the strains

* E. Hug, O. Hubert and M. Clavel are with the LG2MS, URA CNRS 1505, University of Technology of Compiègne, France.

can be explained using potential model theories for the grain oriented alloy in the range [2-8]%. Domain wall bowing theories could successfully be applied to both alloys at the ultimate stage of the strengthening. The relationship between the coercivity and the strengthening displays two linear stages for both 3%SiFe alloys, instead of the three stages ordinarily reported in the case of polycrystalline high-purity iron.

I. INTRODUCTION

The prediction of total core losses in magnetic media used for the manufacture of transformers and rotating electrical machines requires a numerical approach. To this end, standard magnetic characteristics of the materials, i.e. core losses versus flux density and magnetization curve under an ac supply, obtained with classical techniques of measurement (standard Epstein facility or Single Sheet Tester), need to be known with high precision. These standard tests are generally implemented with laminated sheet strips annealed after cutting. Hence, the magnetic properties are expected to be independent of any residual stresses which could exist inside the metal die.

Yet, there is a great difference between direct magnetic measurements on electrical machines and standard characteristics. For some machines, this implies total power losses twice or more higher than losses measured with standard frames, especially for high flux density levels. These differences result from several parameters : electromagnetic factors (distorsion of the wave forms, harmonics, ...) and mechanical factors (residual stresses after punching, elastic stresses in service, ...) in particular.

In the present work, the influence of plastic deformation on the magnetic behaviour of grain oriented (GO) and non oriented (NO) 3% SiFe alloys is investigated. Section 2 describes the magnetic frame used to measure magnetic properties directly on stress-strain test pieces. Experimental results showing the evolution of the magnetic

characteristics with plastic strains are then given. The mechanical behaviour of 3% SiFe alloys submitted to various tensile test levels is presented in section 3. The microstructural aspects (dislocation feature evolution with plastic strain, coupled with magnetic domain structure observations) are reported in section 4. Finally, the validity of some models describing the interactions between dislocations and domain walls and the influence of plastic stresses on coercive field strength are discussed in section 5.

II. MAGNETIC PROPERTIES OF PLASTICALLY STRAINED 3% SiFe ALLOYS

A. Experimental Procedure

Standard apparatus for measuring the magnetic properties of ferromagnetic steel sheets (Epstein frame or Single Sheet Tester) are not able to study stress-strain pieces. A magnetic measurement frame has been then built [1] (Fig.1a). It consists of a ferromagnetic yoke where a magnetic flux $\Phi(t)$ is created by a field winding. This flux crosses over the strained specimen which is held in position at the ends of the yoke. A locking system (screws and springs) ensures a small and constant airgap between the sample and the ferromagnetic frame. The dimensions of the latter have been computed in order to always neglect its reluctancy face to this of the sample. The flux rate variations are detected through a secondary winding concentrated in the middle of the tensile test specimen.

The magnetic frame is supplied with an imposed 50Hz sinusoidal current $i(t)$. The electromotive force $e(t)$ induced in the secondary winding and $i(t)$ are stored. $e(t)$ is then numerically integrate. It gives the magnetic flux inside the sample :

$$\Phi(t) = -\frac{1}{n} \int_0^t e(t) dt \quad (1)$$

with n the number of turns of the secondary winding. The magnetic flux density $B(t)$ is then given by the following relationship :

$$B(t) = \frac{\Phi(t)}{S} \quad (2)$$

S is the cross section of the sample. The Ampere's law is applied along the medium magnetic circuit (Fig. 1b) in order to compute the magnetic field strength $H(t)$:

$$H_y(t)L_y + 2H_a(t)L_a + H(t)L = Ni(t) \quad (3)$$

L is the effective length of the specimen crossed by the flux lines, calculated thanks to a numerical simulation of the frame. L_y and L_a are respectively the medium length of the yoke and the airgap length. This latter can be measured by optical microscopy ($L_a \approx 6\mu\text{m}$ on average). N is the number of turns of the field coil. This experimental system has been numerically validated and it is reliable up to $H = 6000\text{A/m}$. The total flux $\Phi(t)$ is then supposed to be invariant along the magnetic circuit. This allows us to use the following relationships :

$$H_y(t) = \frac{\Phi(t)}{\mu_y(H_y(t))S_y} \quad (4)$$

$$H_a(t) = \frac{\Phi(t)}{\mu_0 S_a} \quad (5)$$

S_y and S_a are respectively the yoke and airgap sections. S_y is thousand time higher than S so H_y is much smaller than H ($H_y \leq 50 \text{ A/m}$). μ_y is also considered as a constant permeability of the yoke estimated as $\mu_y = 1000\mu_0$, with $\mu_0 = 4\pi 10^{-7} \text{ H/m}$.

Consequently, relations (3), (4) and (5) give rise to the magnetic field strength $H(t)$ inside the specimen* :

$$H(t) = \frac{N}{L} \cdot i(t) - \frac{\Phi(t)}{L} \cdot \left(\frac{L_y}{S_y \mu_y} + \frac{2L_a}{S_a \mu_0} \right) \quad (6)$$

The maximum magnetic flux density B_m is plotted against the maximum magnetic field H_m in order to obtain the magnetization curve of the specimen under ac supply excitation. Furthermore, the area of the hysteresis loop is proportional to the total core losses P of the material, for a given value of B_m . coercivity, retentivity and initial permeability are obtained under quasi-static ($f=0.1\text{Hz}$) conditions.

Materials investigated are GO and NO 3%SiFe alloys. Specimens consist in 200mm long, 20mm wide and 0.35mm thick strips cut along the rolling direction of the sheets. They have been annealed (720°C , 2h, $P_{O_2} = 0,027\text{Pa}$) and then plastically deformed at various plastic strain levels ϵ_p , up to fracture. Tensile tests have been performed at room temperature and at a constant plastic rate $d\epsilon_p/dt = 6.67 \cdot 10^{-4} \text{ s}^{-1}$.

B. Experimental Results

* Nevertheless, we have observed that $H(t) \approx (N/L)i(t)$ whatever the magnetomotive strength $Ni(t)$ and the plastic strain level applied to the specimen. The magnetic flux density $B(t)$ is sinusoidal for the lower values of $H(t)$ and become trapezoidal for higher levels.

Figure 2 shows the evolution with ϵ_p of the magnetization curves and the loss characteristics for the two alloys. Plotting various magnetic properties against ϵ_p (Fig.3) shows a marked dependence for low and medium values of magnetic field amplitude i.e. between 0 and 2000 A/m. This phenomenon is weaker when high magnetic field amplitudes are reached.

Simple empirical relations can be found between the main magnetic properties and plastic strains [2], [3]. The maximum magnetic flux density decreases according to the law :

$$B_m = B_{m0}(H_m) \cdot \frac{k_{mc}(H_m)}{k_{mc}(H_m) + \epsilon_p^{n_{mc}(H_m)}} \quad (7)$$

$B_{m0}(H_m)$ is the initial magnetization curve at $\epsilon_p = 0\%$, k_{mc} and n_{mc} are parameters functions of H_m and representative of the material. Furthermore, the following relation gives the increase of the total power losses versus plastic strains :

$$P = P_0(B_m) \cdot [1 + k_p(B_m) \cdot \epsilon_p^{n_p(B_m)}] \quad (8)$$

$P_0(B_m)$ is the initial power loss characteristic. k_p , n_p are parameters depending on B_m and representative of the alloy too. The retentivity of the materials and their initial relative permeabilities μ_{ri} strongly decrease according to :

$$B_r = \frac{B_{r0}}{1 + \epsilon_p^{n_r}} \quad (9)$$

$$\mu_{ri} = \frac{\mu_{ri0}}{1 + \epsilon_p^{n_\mu}} \quad (10)$$

Finally, the coercive field strength markedly increases :

$$H_c = H_{c0} \cdot (1 + \varepsilon_p^{n_c}) \quad (11)$$

B_{r0} , μ_{ri0} and H_{c0} are respectively the values of retentivity, initial permeability and coercive field strength without plastic strains. n_r , n_μ and n_c are constants representative of the studied alloys. Numerical values of the various parameters which appear in relations (7) to (11) can be found in [1], [2].

III. TENSILE TEST BEHAVIOUR OF 3% SiFe ALLOYS

Monotonous stress-strain curves $\sigma(\varepsilon)$ are shown in figure 4 for the two SiFe alloys. Both exhibit a Lüders strain state at the beginning of straining (σ remains constant on a range of deformation L_p , length of the Lüders level). Moreover, materials often exhibit a discontinuity of the yield point $\Delta\sigma_e$.

After the Lüders strain state, classical strengthening is observed. This phenomenon is well marked for the NO alloy and less sensitive for the GO. Non homogeneous deformation occurs after the maximal stress σ_m preceding rupture. This can be characterized by $A\%$, the rupture elongation of the sample.

The true stress-strain curves $\sigma_v(\varepsilon_v)$ follow a classical Ramberg-Osgood law [4] :

$$\sigma_v = C + K_y \cdot \varepsilon_v^n \quad (12)$$

with $C \approx 0$ for weakly alloyed steels, K_y and n are respectively the plastic strength and the strain hardening coefficients. Table 1 summarizes the several mechanical parameters representative of tensile tests carried out on NO and GO alloys.

IV. MICROSTRUCTURAL ASPECTS

Transmission Electron Microscopy observations of strained specimens were performed. Colloid techniques have been also used to observe ferromagnetic domains. Magnetic domain patterns are strongly dependent of the dislocation structure. This microstructural study gives helpful informations about the harmfulness of some dislocation configurations and about the interactions between domain walls and dislocations in 3% SiFe alloys.

A. Behaviour of Dislocations with Plastic Strains

Typical configurations of dislocations for the non oriented alloy were previously reported [2]. For unstrained specimens, the basic dislocation arrangement consists of long screw dislocations lying in a $\{110\}$ glide plane and with a Burgers vector $b=a/2\langle 111 \rangle$. These dislocations are either isolated or get some trend to accumulate close to grain boundaries. Between 0 and 0.5% of plastic strain, a strongly heterogeneous dislocation structure was observed in the Lüders domain. This later structure consists in hexagonal cells with mean size of $26\mu\text{m}$. This structure was no longer observed at higher strains. In the range 1 to 10% of plastic strain roughly homogeneous dislocation structure is observed. In this range, small tangles of relatively low density are progressively created (about $0.1\mu\text{m}$ in length), with isolated glissile dislocations in the channel. Above $\epsilon_p=10\%$, the dislocation structure becomes strongly heterogeneous. Tangles of high density are created, with a typical dimension of $(0.2\mu\text{m}\times 1\mu\text{m})$. In this channel, the dislocation density remains very low.

Similar dislocation structures have been reported for the grain oriented alloy by ourselves and recently for soft steels by Hou and Lee [5]. All these structures are characteristic of the strengthening process of body centered cubic alloys. Only the

critical plastic strains are modified, due to the different rupture elongation of the two alloys. The three main dislocation features are summed up in figure 5.

The average density of statistically stored dislocation were previously computed using a method reported elsewhere [6], [7]. It was observed that the two alloys follow the linear relationship :

$$\rho_d = \rho_{d0} \cdot (1 + \beta \cdot \varepsilon_p) \quad (13)$$

ρ_{d0} is the initial dislocation density ($6 \cdot 10^8$ cm/cm³ for the NO and $2 \cdot 10^8$ cm/cm³ for the GO), β being a constant representative of the alloy.

B. Magnetic Domain Structures and Plastic Strains

Observations of the magnetic domain patterns were carried out on deformed grain oriented samples, thanks to a colloidal method. Several configurations of magnetic domains may be observed [8] with increasing strain levels.

It is well known that grain oriented sheets have a Goss texture that implies boundaries of main domain structures more and less parallel to the easy direction $\langle 001 \rangle$. This main domain structure can be represented by the surface density Ω_1 , following the definition given by Shilling and Houze [9]. When ε_p ranges from 0 to 2% (Lüders strain state of the GO sheet), strong increase of the supplementary structure density happens (this density we may call Ω_2). This secondary structure is composed of reverse spikes of opposite magnetization on grain boundaries, lancet networks or fir-tree patterns. Around 5% of plastic deformation, transverse domains suddenly appear into slab domains and at some grain boundaries. What is more, a relative stabilization of Ω_1 and Ω_2 after this strain rate is noticed. For ultimate values of ε_p , bowing of slab walls occurs and so Ω_2 increases again at the expense of Ω_1 .

A statistical analysis of the magnetic domain structures observed on strained GO samples indicates that the evolution of Ω_1 and Ω_2 versus ε_p clearly shows three distinct stages (Fig.6), each of them corresponding to a typical magnetic domain structure. These experimental results show the role played by the transverse domain structures which counterbalance the increase of the magnetoelastic energy brought with the strengthening process.

Observations of magnetic domain structure on strained NO samples using colloid techniques is very difficult because of the smaller grain size of these alloys (80 μm against 500 μm for GO on average) and the strong initial density of the secondary structure. Measurements of Ω_1 and Ω_2 don't give reproducible results. Nevertheless, bowing of the main domain structure occurs only after 10% of plastic strains, when dislocations tangles of high densities are present in the metallic matrix.

V. DISCUSSION

A. Dislocations / Bloch Walls Interaction Models

1) *Presentation of the models:* The modelling of the movement of domain walls in crystals containing pinning centers like dislocation features remains very difficult. These approaches need a statistical treatment, which generalizes the former models of interaction between one single domain wall and one single dislocation [10], [11], [12], and between one domain wall and an array of dislocations [13], [14]. Typically, the main models may be classified into two categories i.e. the potential models [15], [16] and the domain wall bowing models [17].

In the first category, it is thought that the domain walls are rigid. Local potential energy fluctuations drive their movements. Subjected to an outside magnetic field H , the displacement of a domain wall is function, as first approximation, of two energies : the field energy and the domain wall energy. This latter is generally supposed to be

dependent of the position of the wall. When reversible movements of domain walls occur (Rayleigh zone), the initial relative permeability μ_{ri} is the main magnetic parameter. On the other hand, irreversible displacements of the walls are controlled by the coercive field strength H_c . However, in a real strained crystal, domain wall displacements are perturbed by the elastic stress field of dislocations. The theoretical approach of Kronmüller, Seeger and co-workers [12], [18], [19] shows that H_c may be written as a function of the dislocation density :

$$H_c = C^{te} \cdot \sqrt{\rho_d} \quad (14)$$

and the initial permeability of the material obeys to the law :

$$\mu_{ri} = \frac{C^{te}}{\sqrt{\rho_d}} \quad (15)$$

The product $H_c \cdot \mu_{ri}$ is assumed to be constant to verify the potential theory. Since a linear relation exists between ρ_d and ϵ_p in the range [0-10]% (relation (13)), then $H_c \cdot \mu_{ri}$ must be independant of the applied plastic strain. Using the relations (10) and (11) :

$$H_c \cdot \mu_{ri} = H_{c0} \cdot (1 + \epsilon_p^{n_c}) \cdot \frac{\mu_{ri0}}{1 + \epsilon_p^{n_\mu}} = C^{te} \cdot \frac{1 + \epsilon_p^{n_c}}{1 + \epsilon_p^{n_\mu}} \quad (16)$$

We must have $n_c = n_\mu$ to apply the potential theory to 3%SiFe alloys.

In the second class of models, the dislocation structures act as pinning centers with variable strength amplitudes. Under the influence of an outside magnetic field, the variation of magnetization in the sample is performed by the bowing of the free segments of walls. Irreversible jump occurs for a critical value of the radius of

curvature. Based on this hypothesis, Labush [20] developed a statistical model concerning flexible walls and pinning center density. The author obtains the relationship :

$$H_c = C^{te} \cdot \rho_d^{2/3} \quad (17)$$

Thus, according to relation (13), H_c must be proportional to $\varepsilon_p^{2/3}$ to verify bowing walls models.

2) *Experimental results*: Figure 7 gives the evolution of $H_c \cdot \mu_{ri}$ with ε_p for the GO and NO alloys when a linear relationship between ρ_d and ε_p is verified. An evolution in two stages of $H_c \cdot \mu_{ri}$ against ε_p is observed for the oriented material and a monotonous decrease of $H_c \cdot \mu_{ri}$ with ε_p occurs for the non oriented alloy. Furthermore, fitting H_c against ε_p with the help of relation (7) gives $n_c = 0.23 \pm 0.05$ for the NO alloy and $n_c = 0.18 \pm 0.05$ for the GO alloy. Confrontation of these tendencies with the microstructural investigations gives us the following conclusions (these various effects are listed in figure 8) :

- For Non Oriented Materials : Potential Models do not apply between 0 and 10% of plastic strains because of the variation of the $H_c \cdot \mu_{ri}$ product. Furthermore, bowing models seem more able to explain our experimental results after 10% of plastic strains, but cannot explain the behaviour of the material between 0-10% of plastic strains because relation (17) is here not verified.

- For Grain Oriented Materials : Potential Models do not apply to samples deformed between 0 and 2% (Lüders strain state) because of the variation of the $H_c \cdot \mu_{ri}$ product. between 2 and 8% of plastic strains, $H_c \cdot \mu_{ri}$ remains constant and no bowing of main domain structure is observed: potential models could then successfully be applied.

After $\varepsilon_p=8\%$, bowing of 180° domain walls occurs and then bowing models must be used.

3) *Discussion:* The last results relative to the coercive field strength are based on the hypothesis that dislocation features are the only source of pinning for the domain walls. In fact, the phenomenon could be more complex if grain boundaries are taken into account. In this case, H_c could be written as the sum of two components :

$$H_c = H_{cb} + H_{cd} \quad (18)$$

with H_{cb} an almost constant contribution from grain boundaries and H_{cd} a variable contribution from dislocations. So, $(H_{cb} + H_{cd})\mu_r$ is not constant, while $H_{cd}\mu_r$ can be constant. Nevertheless, our experimental results are related to the total coercive field strength of polycrystalline alloys. The potential models seem hardly applicable in the range of plastic strains where $H_c\mu_r$ is not a constant. In fact, potential models are entirely valid only in the case of strained single crystals [12]. In this case, the displacements of magnetic walls are hindered by the same obstacles (dislocations) and it has been shown that the two models (potential and bowing) are the limit cases of a more general model of interaction [21]. Previous experimental works on polycrystalline Ni and Permalloy have given similar results than those obtained on 3% SiFe alloys [22].

B. Influence of Plastic Stress on Coercive Field Strength

To explain the evolution of magnetic properties with strengthening, several authors prefer to use $\Delta\sigma=\sigma-\sigma_e$ instead of the plastic strain ε_p [23]. We have shown elsewhere that $\Delta\sigma$ is representative of the total strengthening of the alloy at each step of

the straining process [2]. It is interesting to compare the evolution of H_c with $\Delta\sigma$ for our alloys and for high-purity iron as it was determined by Degauque [24] (figure 9).

A variation of H_c following two linear stages for each SiFe alloy is shown. The first stage encountered for high purity iron does not exist in our case. Each stage can be tied to a specific configuration of dislocations. For instance, for the high purity alloy, the first stage ($H_c=c^{te}$) corresponds to isolated and mobile dislocations, the second stage (strong increase of H_c) is associated to small isotropic tangles and isolated dislocations, and the third stage to high dislocation density tangles. For SiFe alloys, the first stage (strong increase of H_c for $\Delta\sigma\approx 0$) corresponds to the cell structure observed on Lüders strain state and the second stage to the formation of tangles. The first stage present for high-purity iron does not exist in 3%SiFe because no configuration of purely isolated dislocations is encountered.

On the other hand, it is worth noting that the evolution of H_c against $\Delta\sigma$ is the same for GO and NO alloys. The magnetomechanical interactions in these alloys are rather complex but seem to be more function of short range interactions than function of the long range ones.

VI. CONCLUSION

In this paper, some experimental results concerning the evolution of magnetic properties of grain oriented and non oriented 3%SiFe alloys have been presented. Experimental laws between magnetic properties and ε_p have been achieved. Correlations between these results, mechanical properties and microstructural observations of dislocations and domain structures have been carried out. It has been shown that the formation of transverse domain patterns counterbalances the increase of

magnetoelastic energy brought with the strengthening. Then, the degradation of magnetic properties is less sensitive.

H_c and μ_{ri} measurements with increasing ε_p have shown that potential model theories do not apply to non oriented SiFe but could explain the magnetic behaviour of grain oriented SiFe in the range [2-8]% of plastic strains. For both materials, domain wall bowing theories seem more able to explain our experimental results at the ultimate stages of deformation. The relationship between coercivity and strengthening displays two linear stages for both 3%SiFe alloys, instead of the three stages reported in the case of a polycrystalline high purity iron [24]. Consequently, the magnetomechanical interactions could be strongly correlated to microstrains surrounding around dislocation features.

These results need to be generalized to different mechanical tests (tensile tests along several directions lying in the sheet plane, fatigue tests, ...) but can be applied with some success to the study of the degradation of magnetic properties of soft magnetic materials after punching. Microhardness measurements can be carried out to obtain the equivalent plastic strain profile near the cutting edge of a punched material [3]. Magnetic properties profiles versus distance from the cutting edge followed, which can be introduced into finite element modelling models of rotating electrical machines. Results concerning the computation of iron losses for a wound rotor synchronous motor and a buried magnet synchronous motor were exposed elsewhere [25]. These simulations have shown a significant majoration of the losses when the punching deformation is taken into account .

REFERENCES

- [1] E. HUG, *Etude des dégradations des propriétés magnétiques d'alliages Fe-3%Si avec les déformations plastiques. Application à la mise en oeuvre des tôles utilisées dans la conception des moteurs électriques*, Thesis, Université de Technologie de Compiègne, 1993.
- [2] E. HUG, M. KANT and M. CLAVEL, "Influence de l'écroissage sur les propriétés magnétiques d'alliages Fe-3%Si non-orientés", *j. phys. III, France*, vol. 4, no. 7, pp. 1267-1284, 1994.
- [3] O. HUBERT and E. HUG, "Influence of plastic strain on magnetic behaviour of non-oriented Fe-3Si and application to manufacturing test by punching", *Mat. Science & Techno.*, vol. 11, pp. 482-487, 1995.
- [4] J. LEMAITRE and J. L. CHABOCHE, *Mécanique des matériaux solides*, Dunod, Bordas, 1988.
- [5] C. K. HOU and S. LEE, "Effect of rolling strain on the loss separation and permeability of lamination steels", *IEEE trans. mag.*, vol. 30, no. 2, pp. 212-216, 1994.
- [6] P.B. HIRSCH, A. HOWIE, R.B. NICHOLSON, D.W. PASHLEY and M.J. WHELAN, *Electron microscopy of thin crystals*, London, Butterworths, 1967.
- [7] F. DUMAS, E. HUG, M. CLAVEL, J.L. ILLE, "Etude du comportement magnétique d'alliages Fe-3%Si non orientés utilisés dans la conception de machines électriques", *j. phys. IV, France*, vol.2, p. C3-47, 1992.
- [8] E. HUG, "Evolution of the magnetic domain structure of oriented 3% SiFe sheets with plastic strains", *J. of Mat. Science*, vol.30, n°17, pp.4417-4424, 1995.
- [9] J. W. SHILLING and G. L. J. HOUZE, "Magnetic properties and domain structure in grain-oriented 3% Si-Fe", *IEEE trans. mag.*, vol. 10, no. 2, pp. 195-223, 1974.

- [10] F. VICENA, "On the influence of dislocations on the coercive force of ferromagnetics", *Czechosl. j. phys.*, vol. 5, pp. 480, 1955.
- [11] M. KLEMAN, "Contribution à l'étude de l'interaction entre une dislocation vis et l'aimantation", *j. phys.*, vol. 29, pp. 329, 1968.
- [12] A. SEEGER, H. KRONMULLER, H. RIEGER and H. TRAUBLE, "Effect of Lattice defects on the magnetization curve of ferromagnets", *j. appl. phys.*, vol. 35, no. 3, pp. 740-748, 1964.
- [13] W. F. J. BROWN, "The effect of dislocations on magnetization near saturation", *Phys. Rev.*, vol. 60, pp. 139, 1941.
- [14] W. F. J. BROWN, "Dislocations, cavities and the approach to magnetic saturation", *Phys. Rev.*, vol. 82, no. 1, pp. 94, 1951.
- [15] C.-W. CHEN, *Magnetism and metallurgy of soft magnetic materials*, E.P. Wohlfarth Editor, North-Holland, 1977.
- [16] D.C. JILES, *Introduction to magnetism and magnetic materials*, Chapman & Hall, 1991.
- [17] H. D. DIETZE, "Theorie der Blochwandwölbung mit Streufeldeinfluß", *Zeit. Phys.*, vol. 149, pp. 276-298, 1957.
- [18] H. KRONMÜLLER, "Statistical theory of Rayleigh's law", *Zeit. Ang. Phys.*, vol. 30, no. 1, pp. 9-13, 1970.
- [19] H. KRONMÜLLER, "Magnetic techniques for the study of dislocations in ferromagnetic materials", *Int. j. of non destr. test.*, vol. 3, pp. 315, 1972.
- [20] R. LABUSCH, "Calculation of the critical field gradient in type II superconductors", *Cryst. Lat. Def.*, vol. 1, pp. 1-16, 1969.
- [21] H.R. HILZINGER and H. KRONMÜLLER, "Statistical theory of the pinning of Bloch walls by randomly distributed defects", *J. Magn. Magn. Mater.*, vol.2, pp.11-17, 1976.

- [22] O. BOSTANJOGLO, R. LIEDTKE and A. OELMANN, "Microscopical test of current theories of magnetic wall motion", *Phys. Stat. Sol.*, vol.(a), n°24, pp.109-113, 1974.
- [23] B. ASTIE, J. DEGAUQUE, J. L. PORTESEIL and R. VERGNE, "Predictions of the random potential energy models of domain wall motion : an experimental investigation on high-purity iron", *J. mag. mag. mat.*, vol. 28, pp. 149-153, 1982.
- [24] J. DEGAUQUE, "Les pertes d'énergie dans les ferromagnétiques métalliques doux : origines physiques", *Mém. Et. Scient., Rev. Métal.*, janv., pp. 5-23, 1985.
- [25] E. HUG, F. DUMAS, J. M. BIEDINGER and M. CLAVEL, "Influence des déformations plastiques sur le comportement magnétique d'alliages fer-silicium", *Rev. Métal. - CIT/Sc. Gen. Mat.*, dec., pp.1857-1866, 1994.

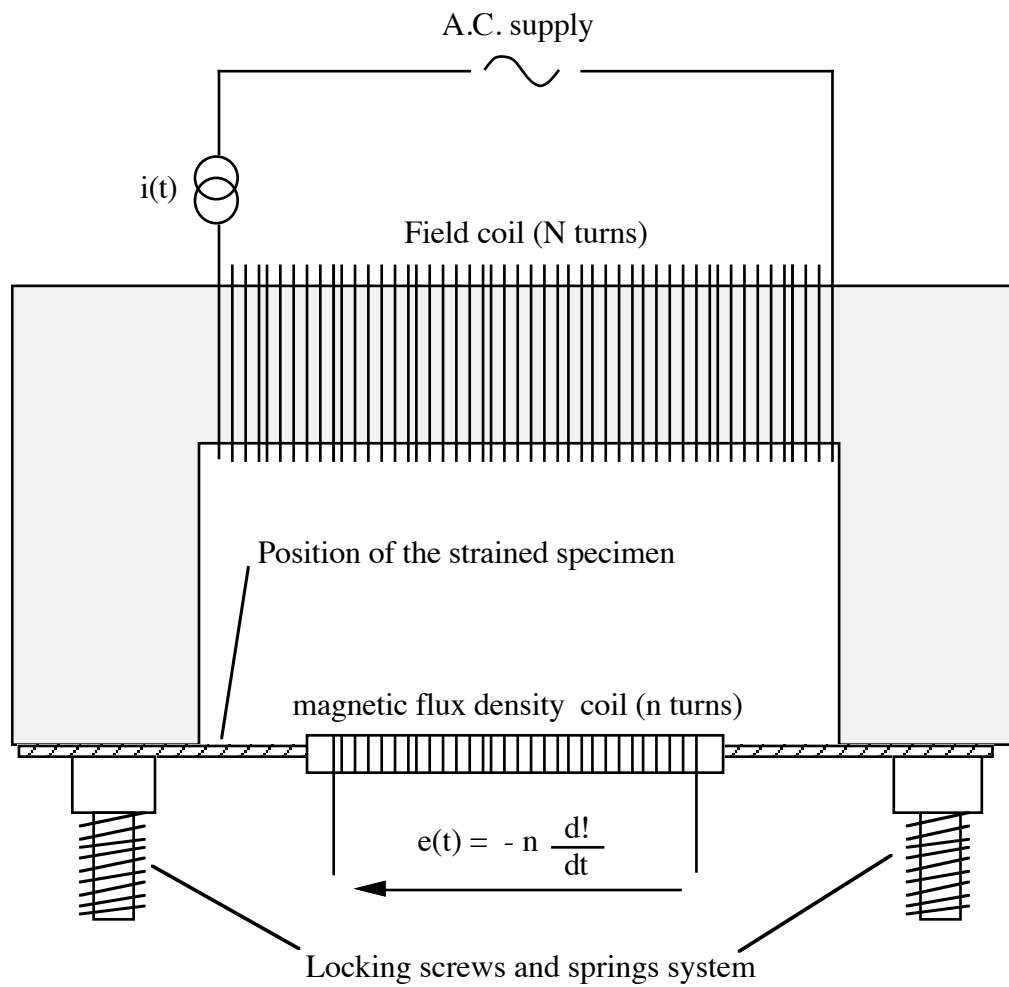


FIGURE 1(a)

Author : E. HUG

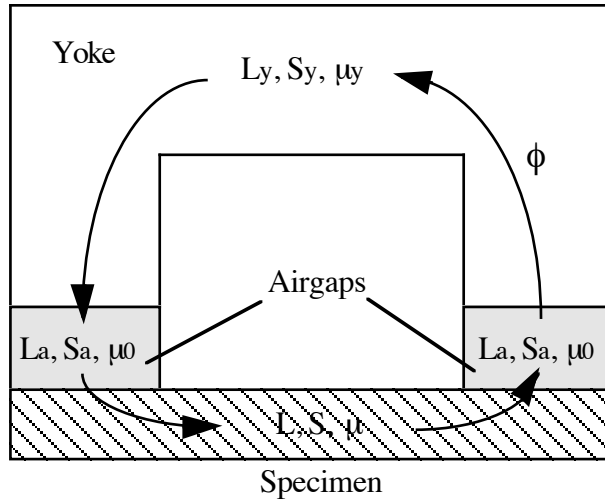
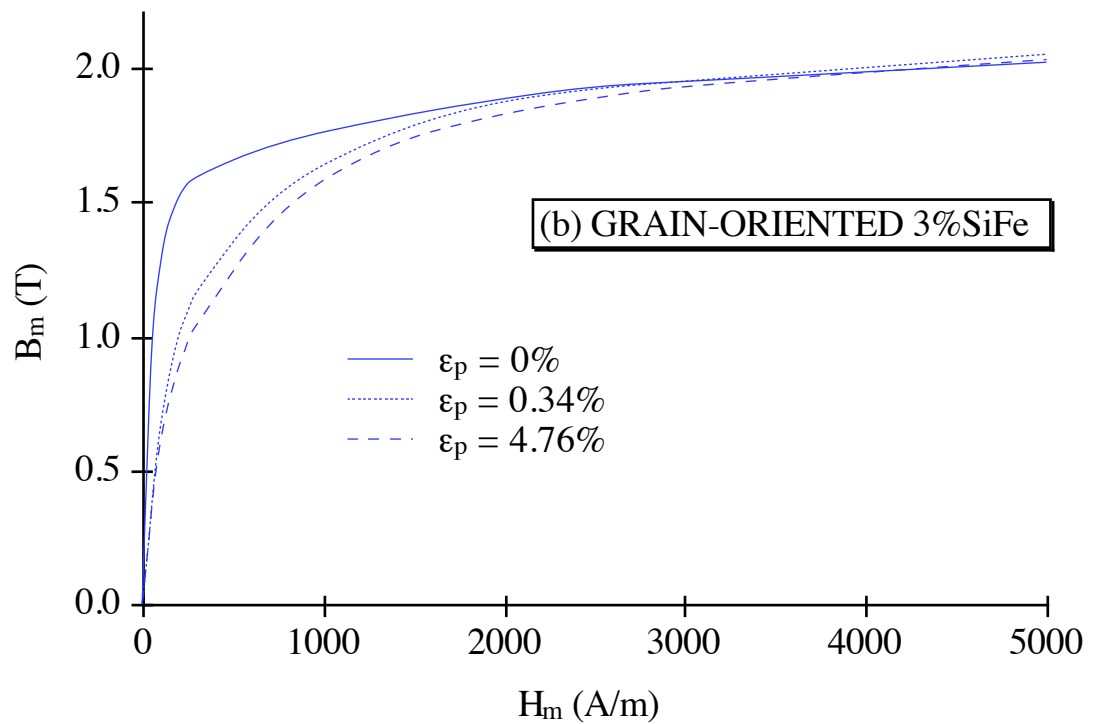
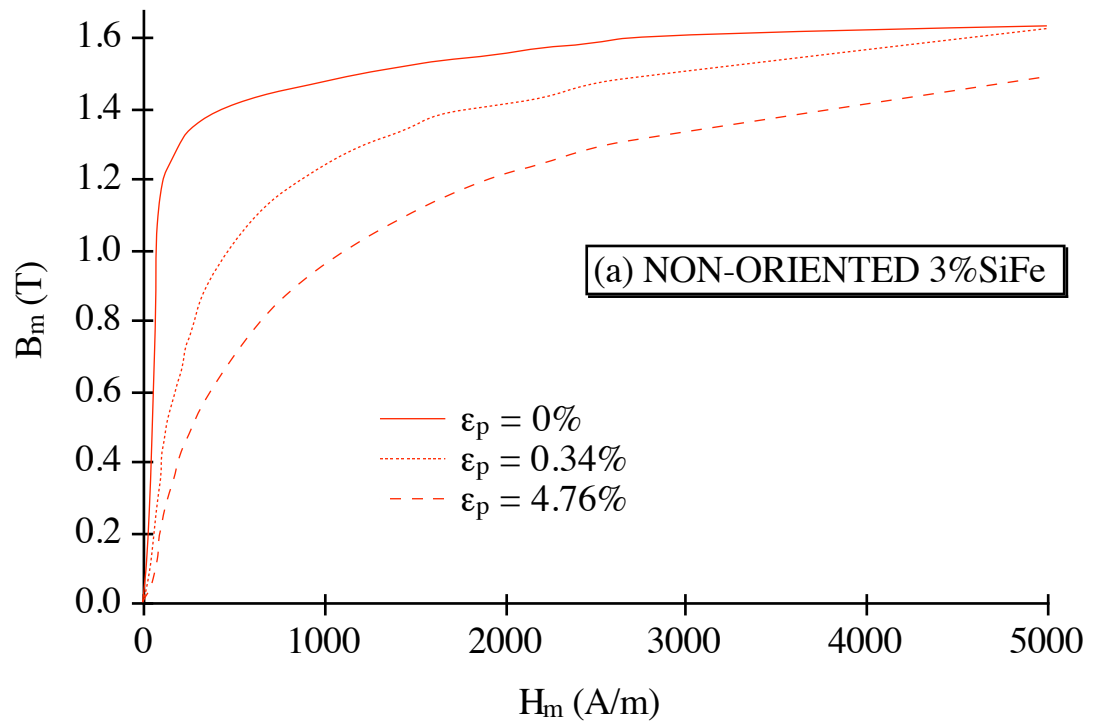


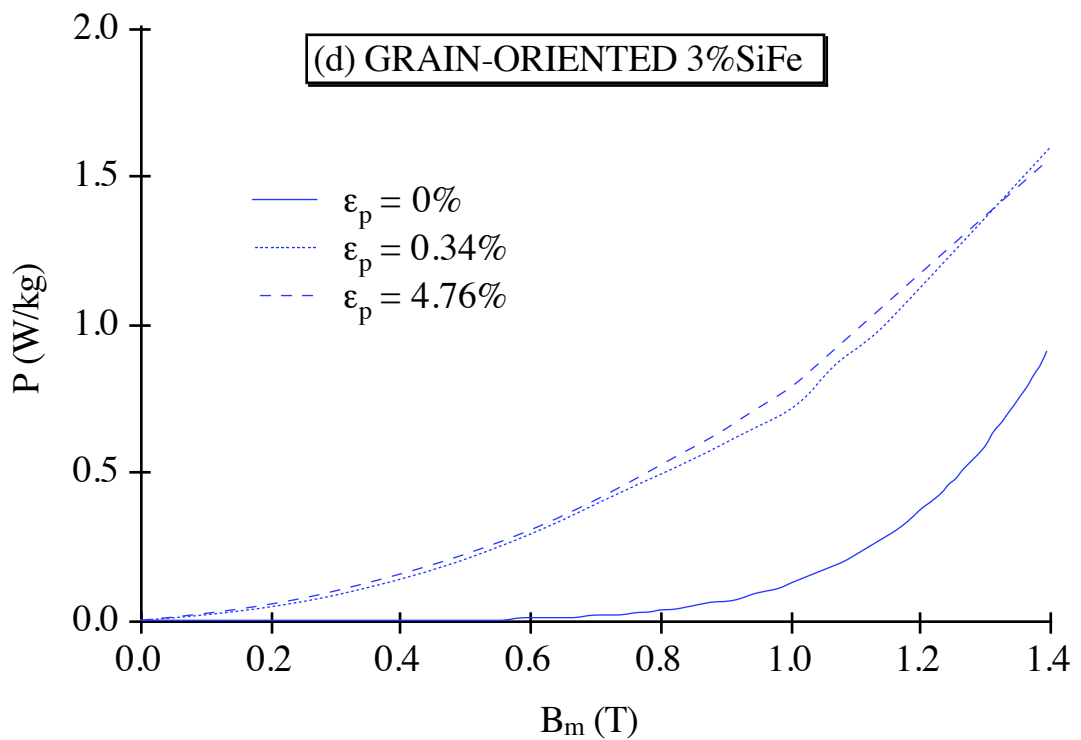
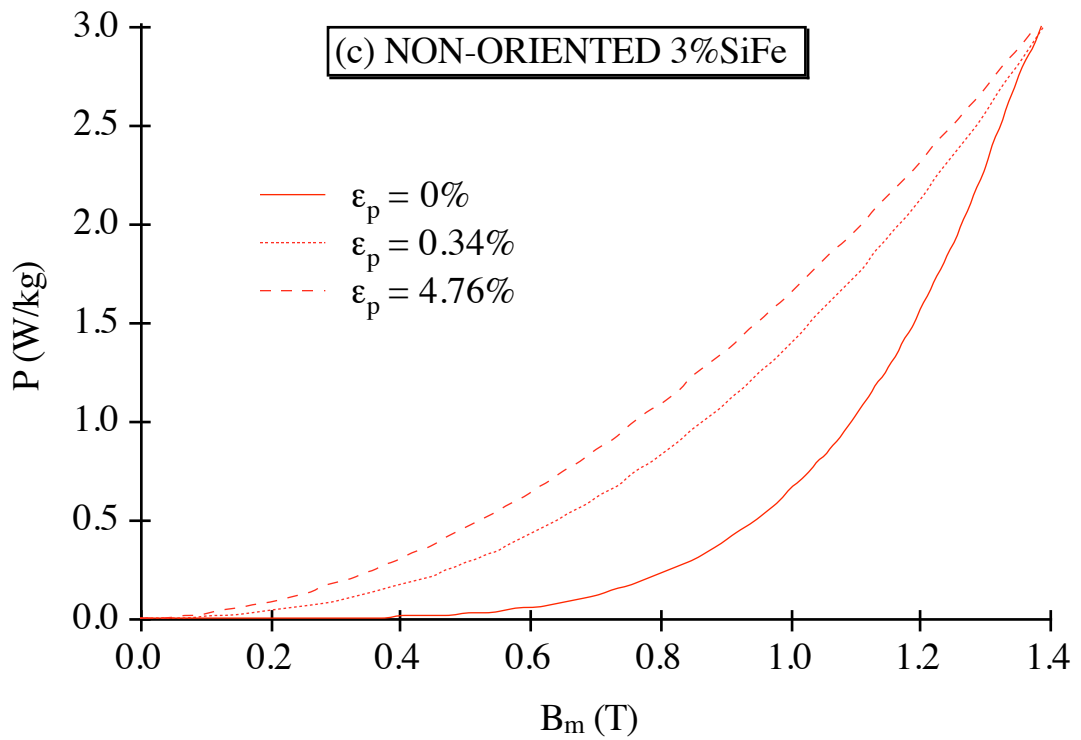
FIGURE 1(b)

Author : E. HUG



FIGURES 2(a) and 2(b)

Author : E. HUG



FIGURES 2(c) and 2(d)

Author : E. HUG

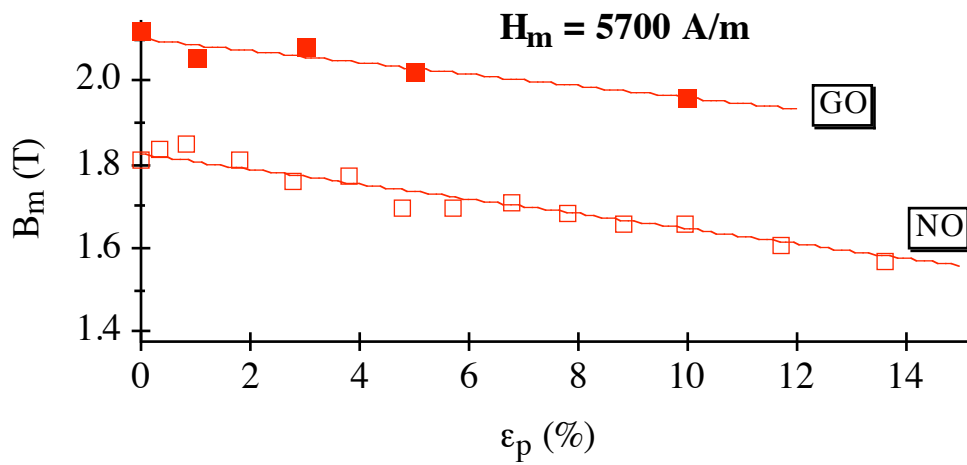
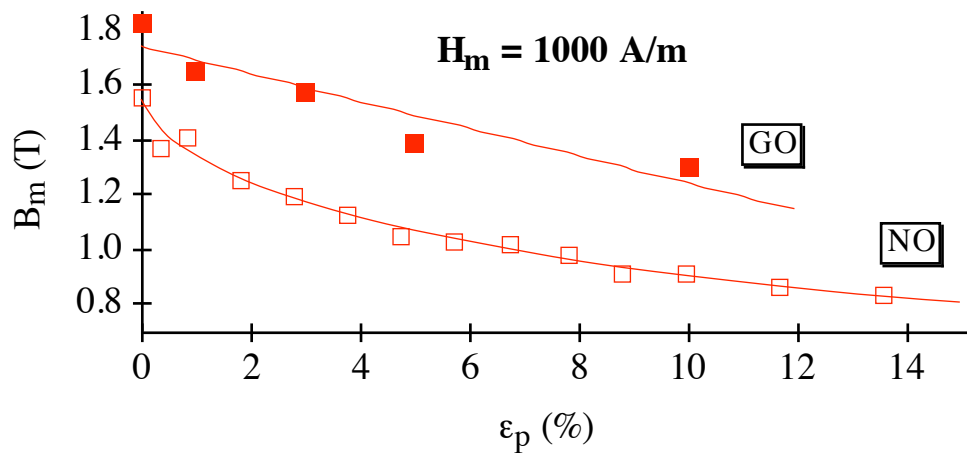
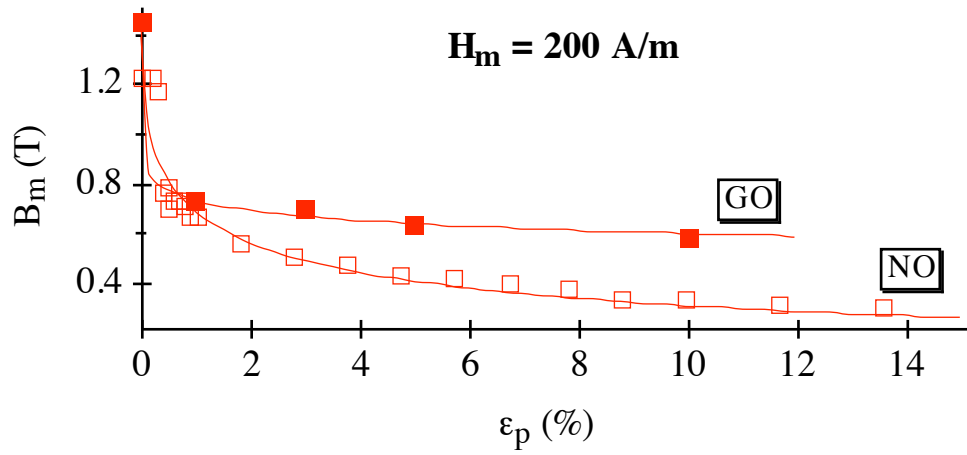
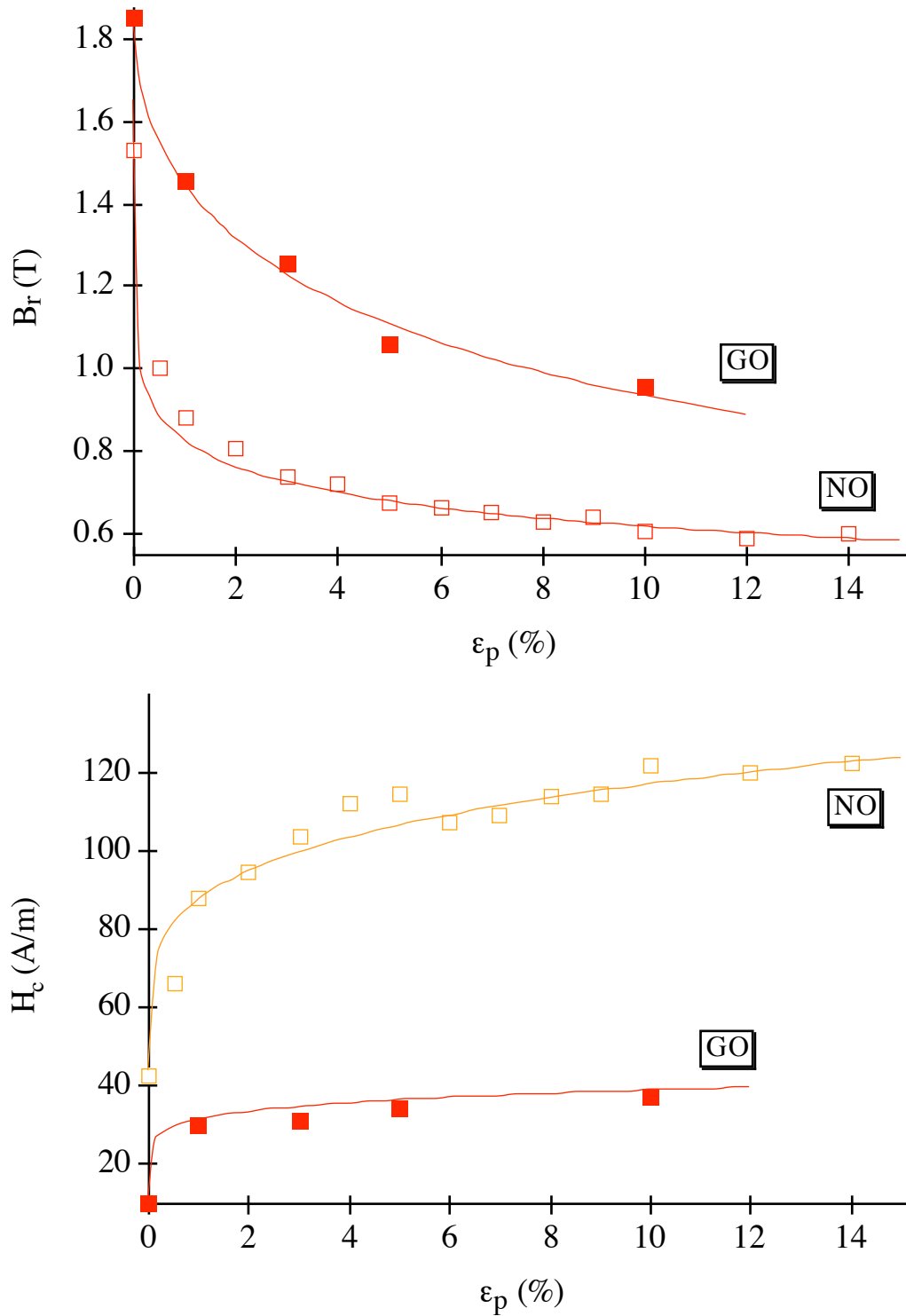


FIGURE 3(a)

Author : E. HUG



FIGURES 3(b) and 3(c)

Author : E. HUG

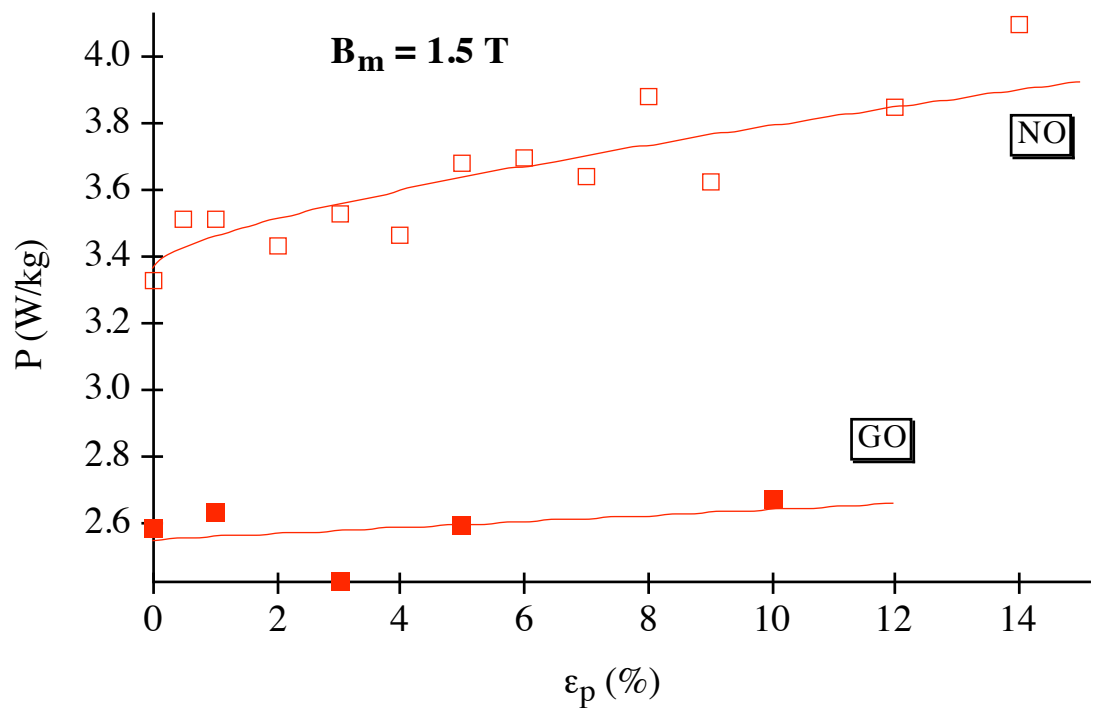
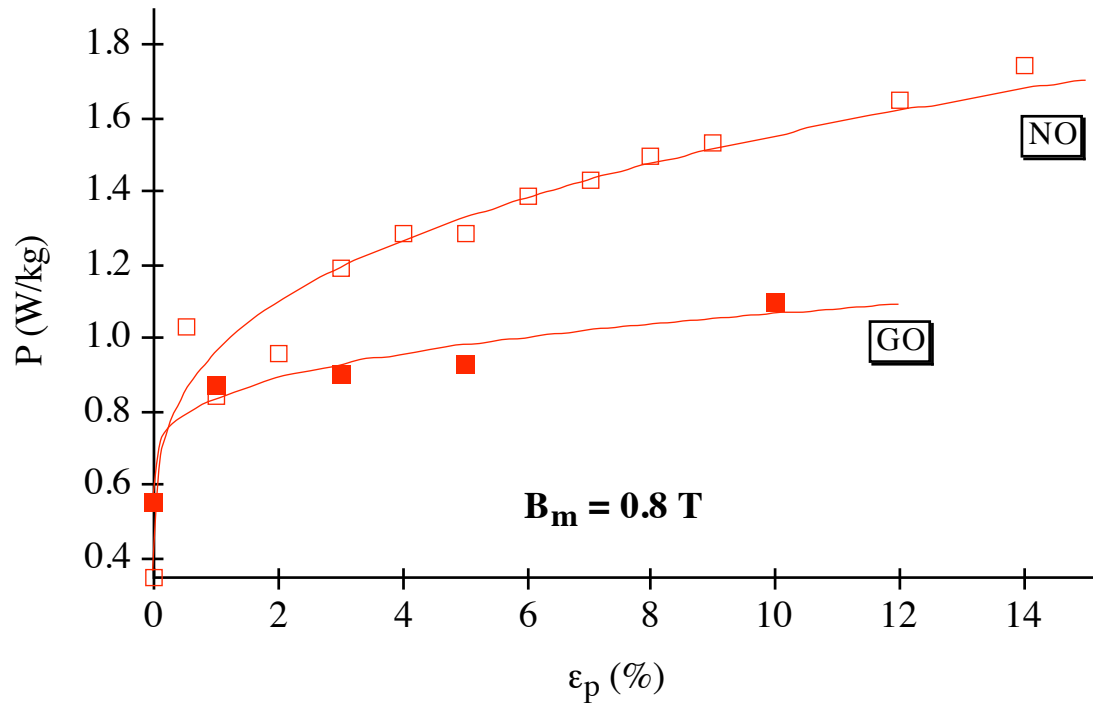


FIGURE 3(d)

Author : E. HUG

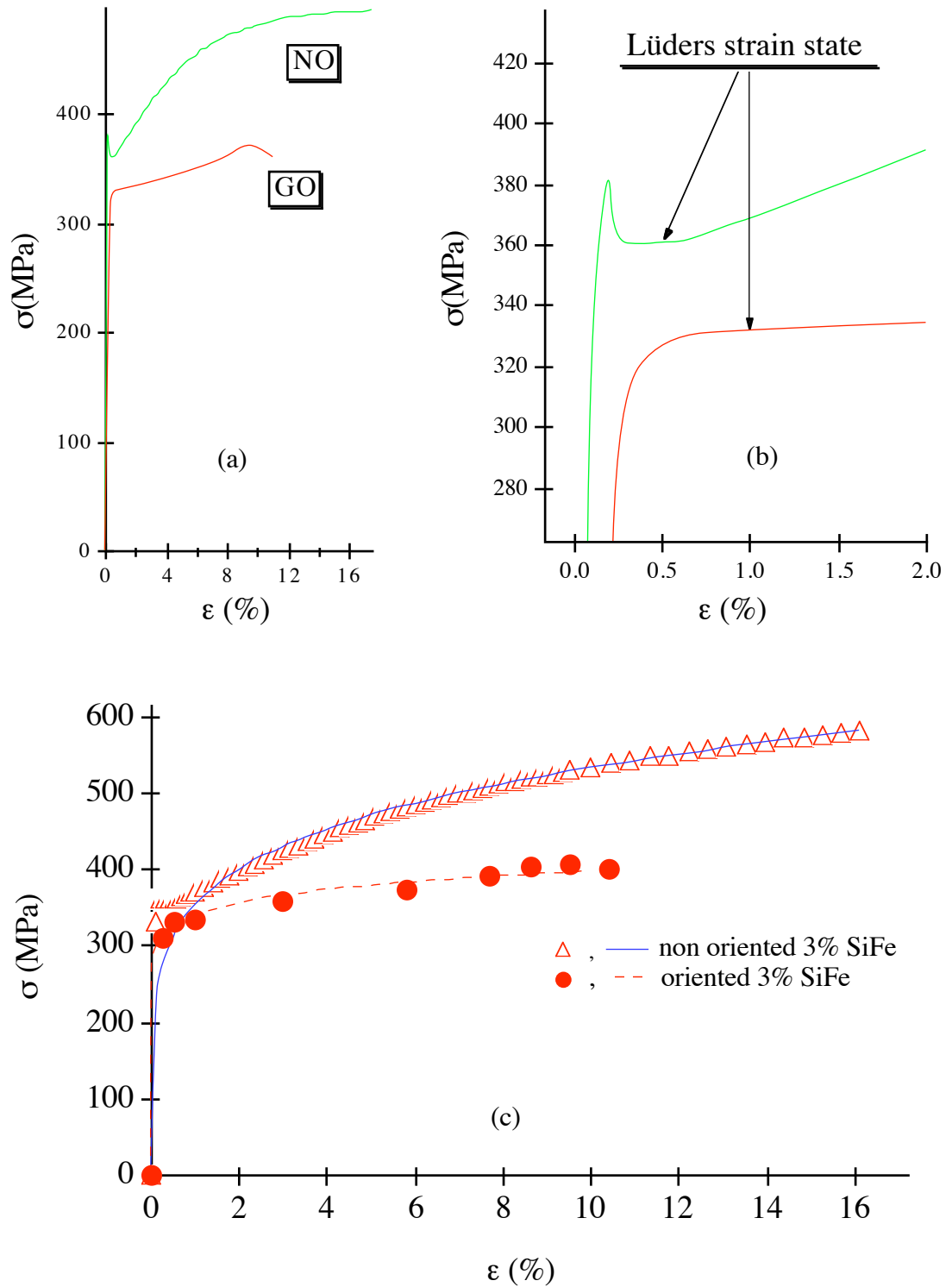


FIGURE 4

Author : E. HUG

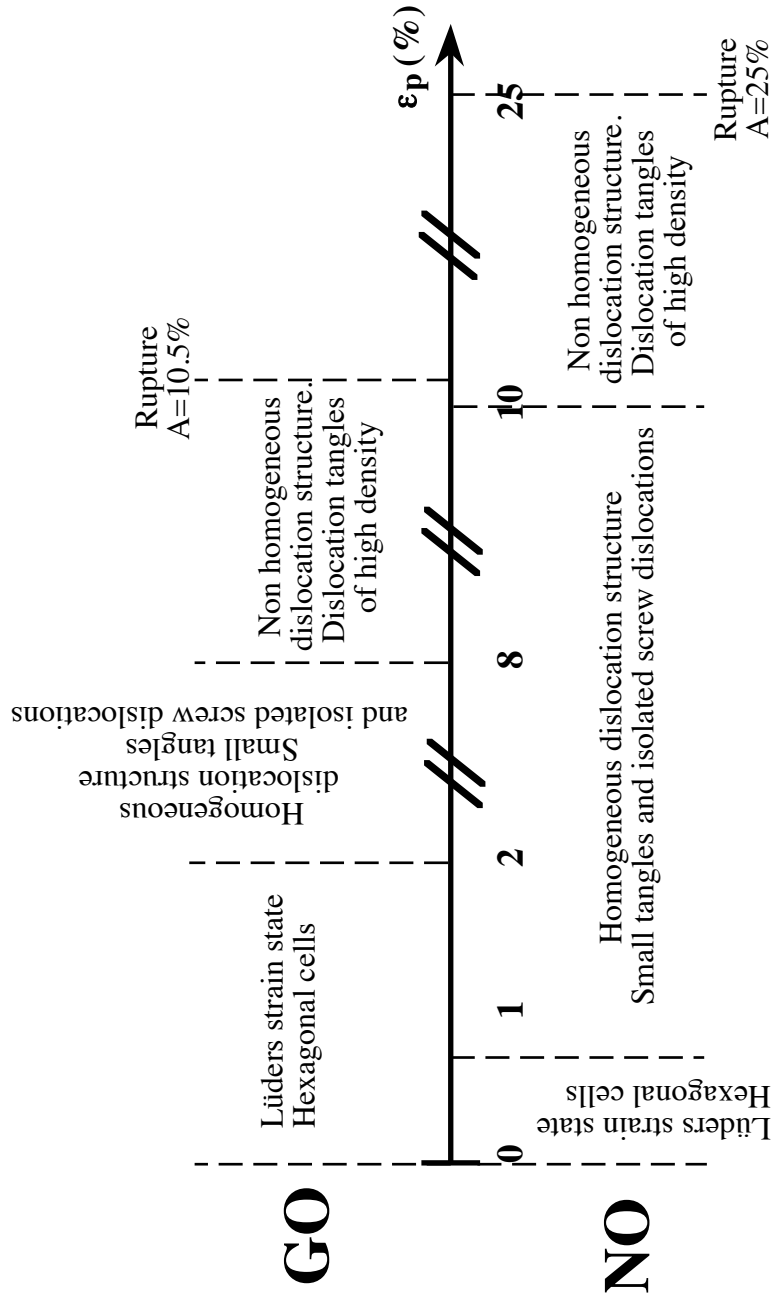


FIGURE 5

Author : E. HUG

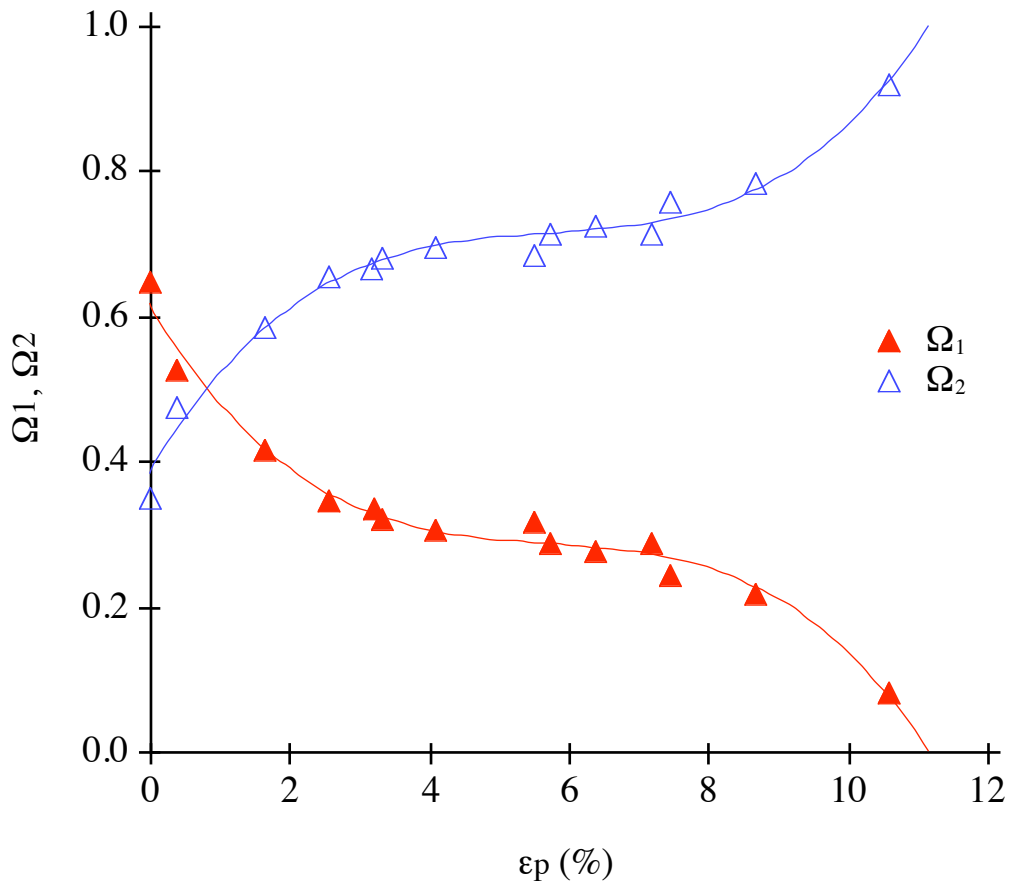


FIGURE 6

Author : E. HUG

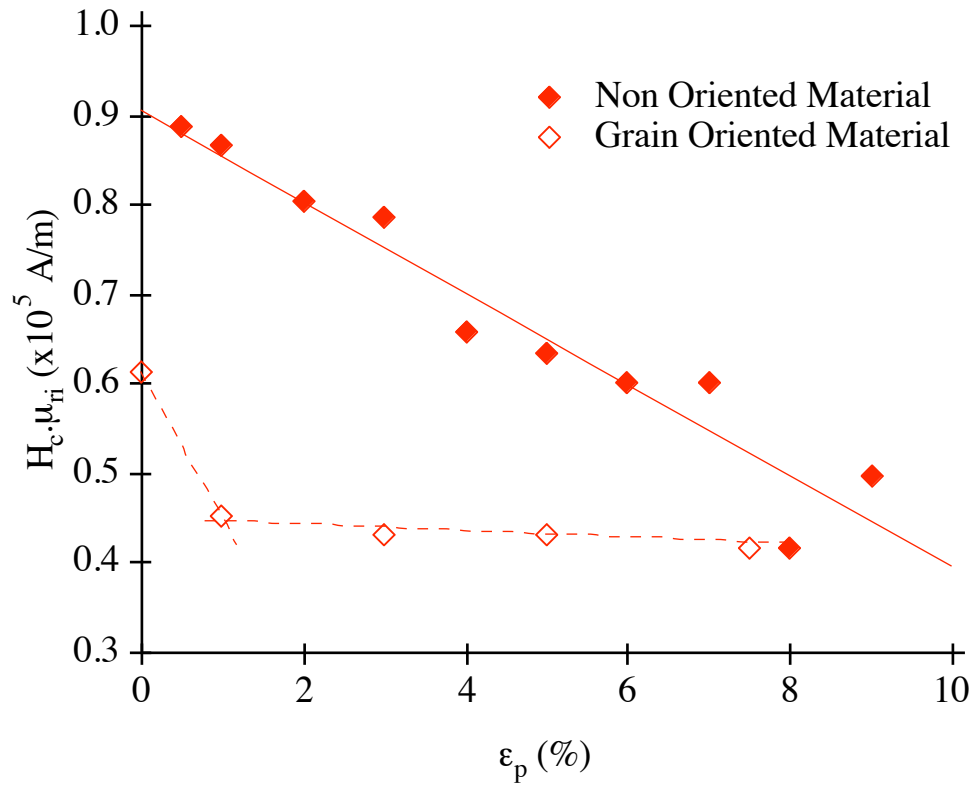


FIGURE 7

Author : E. HUG

GRAIN-ORIENTED 3% SiFe ALLOYS												
Models	None	Potential Models	Bowing Models									
H _c (ε _p)		H _c = H _{c0} (1 + ε _p) ^{nc} nc = 0.18±0.05										
H _c .μ _{ri}	↗	Constant										
Magnetic Domain Structure	↗ Ω ₂ No Bowing	Transverse Domain Structure No Bowing Ω ₁ and Ω ₂ are constants	Bowing of Main Domain Walls Ω ₂ increasing									
Dislocation Structure	Lüders strain state Hexagonal cells	Homogeneous Dislocation Structure ρ _d = ρ _{d0} .(1 + ε _p)	Non Homogeneous Dislocation Structure									
Plastic Strain (%)	1	2	3	4	5	6	7	8	9	10	11	
	1	2	3	4	5	6	7	8	9	10	11	
Dislocation Structure	Lüders	Homogeneous Dislocation Structure ρ _d = ρ _{d0} .(1 + ε _p)		Homogeneous Dislocation Structure ρ _d = ρ _{d0} .(1 + ε _p)		Homogeneous Dislocation Structure ρ _d = ρ _{d0} .(1 + ε _p)		Homogeneous Dislocation Structure ρ _d = ρ _{d0} .(1 + ε _p)		Non Homogeneous Dislocation Structure		
		No Bowing of Main Domain Walls		No Bowing of Main Domain Walls		No Bowing of Main Domain Walls		No Bowing of Main Domain Walls		Bowling of Main Domain Walls		
H _c .μ _{ri}												
H _c (ε _p)		H _c = H _{c0} (1 + ε _p) ^{nc} nc = 0.23±0.05										
Models		None	Bowing Models									
NON-ORIENTED 3% SiFe ALLOYS												

FIGURE 8

Author : E. HUG

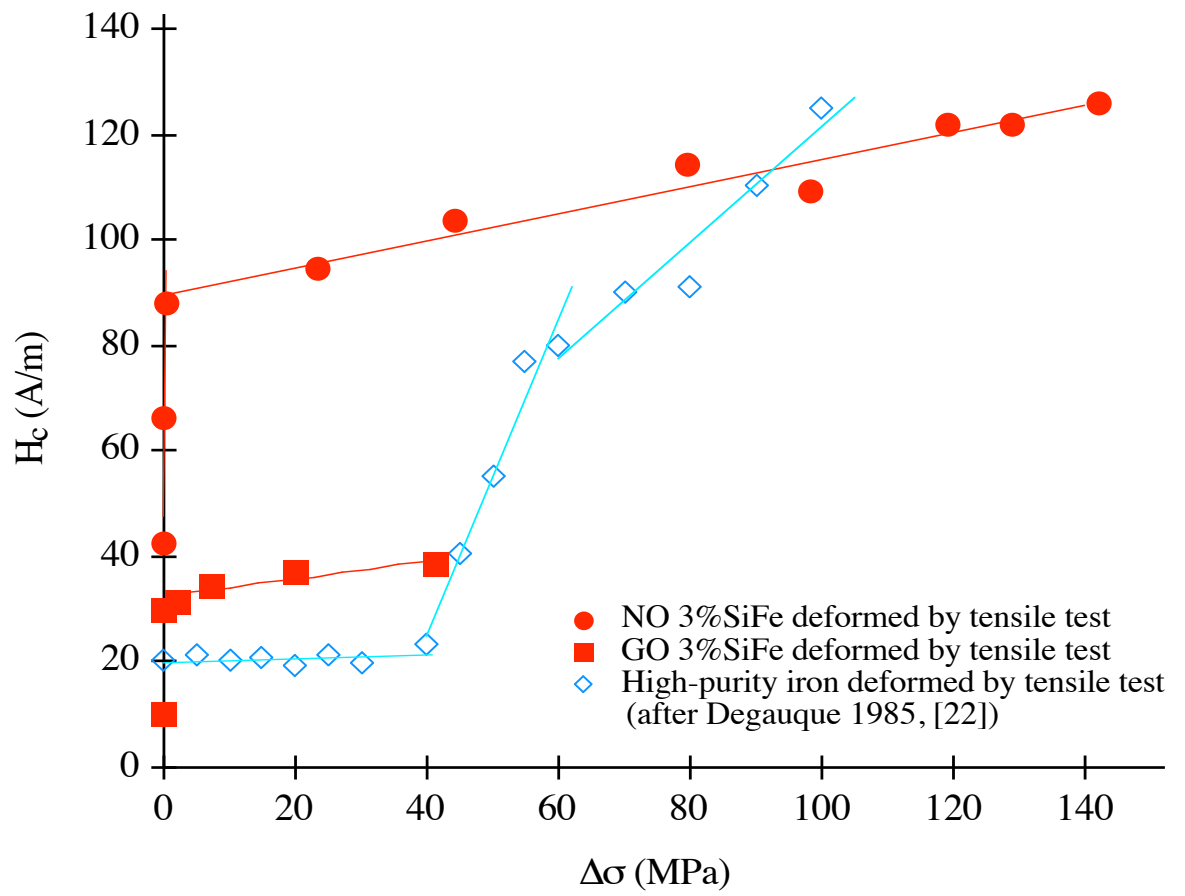


FIGURE 9

Author : E. HUG

	σ_e (MPa)	$\Delta\sigma_e$ (MPa)	σ_m (MPa)	A (%)	L_p (%)	K_y (MPa)	n
NO	360	10	495	25	0.2	350	0.181
GO	290	4.5	365	10.5	1.8	340	0.068

TABLE 1**Author : E. HUG**

FIGURE CAPTIONS LIST

Figure 1 : Principle of magnetic properties measurements on stress-strain test pieces. (a) The experimental frame ; (b) corresponding magnetic circuit.

Figure 2 : Magnetic properties of non oriented and grain oriented 3%SiFe samples with various plastic strain levels. (a) magnetization curves for NO alloys ; (b) magnetization curves for GO alloys ; (c) loss characteristics for NO alloys ; (d) loss characteristics for GO alloys (experimental conditions of magnetic tests are given in text).

Figure 3 : Relationship between magnetic properties and plastic strain levels for NO and GO SiFe alloys. (a) induction versus ϵ_p for several values of the applied magnetic field ; (b) retentivity versus ϵ_p ; (c) coercive field strength versus ϵ_p ; (d) power losses versus ϵ_p for various induction levels.

Figure 4 : Tensile test properties of NO and GO SiFe alloys. (a) monotonous stress-strain curves ; (b) Lüders strain state ; (c) rational stress-strain curves and Ramberg-Osgood models.

Figure 5 : Typical dislocation patterns with plastic strains for NO and GO alloys.

Figure 6 : Relationship between the surface densities Ω_1 , Ω_2 and plastic strain levels.

Figure 7 : Product $\mu_{ri}.H_c$ plotted against ϵ_p , GO and NO alloys. Linear relationship between plastic strains and dislocation density.

Figure 8 : Abstract of the experimental results concerning dislocation structures, magnetic domain patterns, coercivity and $(H_c.\mu_{ri})$ product for NO and GO alloys at various stages of plastic deformation. Validity of potential and bowing models for domain walls / dislocations interactions.

Figure 9 : Evolution of H_c with the plastic stress level $\Delta\sigma$ for NO and GO alloys, and for high purity iron as determined in [22].

TABLE CAPTIONS LIST

Table 1 : typical values of the mechanical parameters representative of the tensile test behaviour of the two SiFe alloys.

CORRESPONDENCE AUTHOR

Eric HUG

Division Matériaux - Dept Génie Mécanique, Laboratoire LG2MS, URA CNRS 1505.
Université de Technologie de Compiègne, BP 649, 60206 COMPIEGNE Cedex
FRANCE

Telephone : (33) 44.23.44.23, poste n°4255.

Fax : (33) 44.20.48.13

COAUTHORS

• **Olivier HUBERT**

Division Electromécanique - Dept Génie Mécanique.
Université de Technologie de Compiègne, BP 649, 60206 COMPIEGNE Cedex
FRANCE

• **Michel CLAVEL**

Division Mécanique - Dept Génie Mécanique, Laboratoire LG2MS, URA CNRS 1505.
Université de Technologie de Compiègne, BP 649, 60206 COMPIEGNE Cedex
FRANCE